Journal of Nuclear Materials 395 (2009) 30–36

Contents lists available at ScienceDirect

Journal of Nuclear Materials

journal homepage: www.elsevier.com/locate/jnucmat

Tensile and stress corrosion cracking behavior of ferritic–martensitic steels in supercritical water

Pantip Ampornrat *, Gaurav Gupta, Gary S. Was

Nuclear Engineering and Radiological Sciences, University of Michigan, 2355 Bonisteel Blvd., Ann Arbor, MI 48109, USA

ARTICLE INFO

Article history:
Received 18 September 2009
Accepted 27 September 2009

PACS:
28.52.Fa

ABSTRACT

Tensile and stress corrosion cracking behavior of ferritic–martensitic steels in supercritical water were studied in order to evaluate the suitability of these steels for supercritical water nuclear reactor concept. The ferritic–martensitic steels tested in this study consisted of T91, HCM12A, HT-9, weld T91, and weld HCM12A. A series of constant extension rate tensile (CERT) tests at a strain rate of 3×10^{-7} s^{-1} were conducted in supercritical water over a temperature range of 400–600 °C and pressure 24.8 ± 0.07 MPa. CERT tests in argon and in supercritical water with 100 and 300 appb dissolved oxygen also were performed at 500 °C to compare the effect of environment. The results show that HT-9 exhibited the highest yield and maximum stresses, followed by HCM12A, and T91. The reduction in area of T91 is the highest, followed by HCM12A, and HT-9. Temperature has a great effect on tensile behavior of these steels. An increase in test temperature from 400 to 600 °C reduces the yield stress by ~50%. Both T91 and HCM12A weld steels exhibited a slightly lower yield and maximum stresses than the base steels. Increased dissolved oxygen in the water resulted in a significant reduction of ductility. Fractography showed that all of the specimens exhibited ductile rupture except for HT-9 that showed evidence of intergranular cracking. Intergranular cracking in HT-9 is affected by temperature and oxygen concentration in supercritical water.

© 2009 Elsevier B.V. All rights reserved.

1. Introduction

The supercritical water-cooled reactor (SCWR) is one of the Generation IV advanced nuclear reactor concepts that utilizes water in the supercritical state ($T > 374$ °C, $P > 22.1$ MPa) in a direct, once-through mode. Operation above the critical pressure eliminates boiling, so the coolant remains in single-phase. Viability of the concept requires operation at temperatures up to 620 °C, at pressure greater than 22.1 MPa and core materials that can withstand neutron doses of 15–30 dpa ($E > 1$ MeV) [1,2]. One of the major problems in development of the SCWR is the lack of data on materials behavior in supercritical water (SCW). Among the most important requirements is resistance to corrosion and stress corrosion cracking (SCC) under these conditions. The purpose of this study is to evaluate the stress corrosion cracking behavior of candidate ferritic–martensitic (F–M) steels T91, HCM12A and HT-9 in SCW.

F–M steels are candidates for structural components in the SCWR by virtue of their performance in supercritical fossil plants and the numerous advantages they have over austenitic stainless steels, such as higher thermal conductivity, lower susceptibility to SCC and reduced swelling under irradiation. However, F–M steels have limitations due to high corrosion rates, low creep strength at high temperatures, and radiation embrittlement at low temperatures [3–5].

F–M steels were developed to have high creep rupture strength at elevated temperature and high pressure [3]. F–M steel T91 (9Cr–1MoVNb) has been extensively used for header and steam pipes in ultra supercritical fossil plants operating up to 593 °C [6]. Since 9Cr steels are limited by oxidation resistance, 12Cr steels such as HT-9 have been considered. HCM12A is an advanced version of HT-9 with slightly reduction Cr concentration (~11% Cr) and additions of W and Cu to improve the weldability and creep strength.

This paper focuses on tensile and SCC properties of F–M steels in SCW. The CERT tests were conducted at a slow strain rate (3×10^{-7} s^{-1}) in deaerated SCW at 400, 500 and 600 °C. CERT tests were also conducted in argon, and in SCW containing 100 and 300 appb dissolved oxygen at 500 °C to determine the effect of dissolved oxygen on SCC.

2. Experiment

2.1. Materials and sample fabrication

Three F–M steels: T91, HCM12A, and HT-9 were used in the as-received (normalized and tempered) condition. The heat treatment condition was selected for each steel in order to obtain the

* Corresponding author. Tel.: +1 734 936 0266; fax: +1 734 763 4540.
E-mail address: pantipam@umich.edu (P. Ampornrat).

0022-3115/$ - see front matter © 2009 Elsevier B.V. All rights reserved.
doi:10.1016/j.jnucmat.2009.09.012

optimum microstructure of phase, precipitation and grain size. The chemical compositions in wt.% and heat-treatments are given in Table 1. The microstructure of all three steels consisted of tempered martensite laths forming subgrains in a ferrite matrix, with (V, Nb)-carbonitrides precipitated mainly on dislocations within the subgrains, and $M_{23}C_6$ precipitated on the prior austenite grain (PAG) boundaries and on subgrain boundaries [7]. The major difference in the three F–M steels tested in this study is their PAG size as reported in previous papers; 9, 13.5, and 50 μm for T91 [7], HCM12A [8], and HT-9 [9], respectively.

Samples in the form of round tensile bars 39 mm long with threaded ends, a gage length of 21 mm and square cross-section of 2 mm × 2 mm were fabricated via electric discharge machining (EDM). The SCC bars were mechanically polished using SiC paper FEPA P#4000 (US grit 1200) and then electropolished in a solution of perchloric acid (10%) and methanol at −30 °C with an applied voltage of 35 V for 5–20 s to obtain a mirror finish. Electropolishing ensured the removal of the remelt layer from the EDM process, as the thickness of the remelt layer is ~5 μm on each side, while ~70 μm were removed by polishing on each side.

2.2. Weld samples

To study the effect of welds in T91 and HCM12A, plates were joined by Gas-Tungsten-Arc-Weld (GTAW) at Idaho National Laboratory (Courtesy of Dr. James Cole). To avoid hydrogen cracking, the steel plates were first pre-heated to 250 °C followed by GTAW using P91 (Blue Max LNT 9Cr®) filler. The composition of the filler is listed in Table 1. After welding, the joined pieces were air cooled. A post-weld heat treatment was conducted at 750 °C for 3 h followed by furnace cooling. The post-weld heat treatment was necessary to obtain the proper weld structure and adequate toughness. The surface oxide layer developed during the heat treatment was removed by machining the top face of the plate flat. Fig. 1 shows how the SCC bars were machined through the thickness of the weld and across the width of the plate.

During welding, austenite forms in the heat affected zone (HAZ) and grain coarsening occurs close to the fusion boundary. After cooling, the austenite transforms to martensite, and sometimes the δ-ferrite phase remains at the grain boundary [3]. Since δ-ferrite can cause brittleness, post-weld heat treatment is required to diminish this phase. Grain size in HAZ of welded T91 increased to 20–30 μm, and 17–25 μm in welded HCM12A.

Although this paper will report on the tensile and SCC behavior of samples in the welded and heat treated condition, all welded samples were proton irradiated on one side for another study (see Ref. [7] for details). However the irradiation did not affect the cracking behavior on the un-irradiated side, nor did it affect the stress–strain behavior, which will be discussed in Section 3.2.

2.3. CERT experiments

CERT tests were conducted in a multi-sample supercritical water system at the University of Michigan [4]. To study the role of temperature, experiments were conducted in the range of 400–600 °C in deaerated SCW (DSCW). During exposure, the temperature inside the autoclave was controlled to within ±5 °C of the target temperature. The pressure was maintained between 24.1 and 24.8 ± 0.07 MPa. High purity water of conductivity 0.06 μS/cm was used as the feedwater. The system was maintained at the test temperature without straining for approximately 24 h, to allow the outlet conductivity to stabilize below 0.1 μS/cm. The tensile samples were strained at a rate of 3×10^{-7} s^{-1}. In the deaerated condition, the dissolved oxygen (DO) concentration was maintained below 10 appb by purging argon gas through the column continuously. In controlled-oxygen experiments, argon gas was mixed with oxygen to achieve 100 ± 10 or 300 ± 20 appb DO in the water. The inlet and outlet conductivities were maintained as low as possible using a flow rate greater than 50 ml/min in each experiment. Outlet conductivity was at or below 0.10 μS/cm in all deaerated tests, but increased well above this level in controlled-oxygen experiments, Table 2. Additional CERT tests were conducted in argon on HT-9 to isolate the effect of environment on the SCC susceptibility. Because the experiments were conducted at a pressure of 24.1–24.8 MPa, the total stress applied to the sample is the sum of the stress applied by the motor and that due to the system pressure [10]. The latter is approximately 100 MPa. The experimental results were reported with 2.58σ, where σ is standard deviation of measurement (square root of measured value), covering 99% of confidential interval.

2.4. Fractography

Following CERT tests, scanning electron microscopy (Philips XL-30) was used to characterize the fracture surfaces and to determine the amount of cracking on the sample gage sections. Crack depth was determined from cross-sections of SCC samples prepared by mounting in an epoxy resin followed by mechanical polishing. The mounted specimens were etched in a solution of 1 part HCl to three parts HNO_3 in order to observe the grain boundaries. The cracks were investigated in SEM in both secondary and back scattered electron modes. The crack depth was measured from the deepest crack to the interface of inner and outer oxide (since it is the original

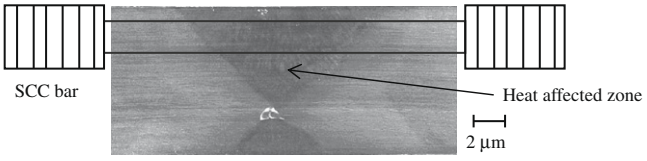

Fig. 1. SCC bar was machined through the thickness of the weld across the width of the SCC bar.

Table 1
Composition and heat treatment of T91, HCM12A, and HT-9.

Alloy	Chemical composition (wt.%)															
	C	Mn	P	S	Si	Ni	Cr	Mo	Cu	N	Co	Ti	Nb	Al	V	W
T 91[a]	0.10	0.45	0.009	0.003	0.28	0.21	8.37	0.90	0.17	0.048			0.076	0.022	0.216	
HCM12A[b]	0.11	0.64	0.016	0.002	0.27	0.39	10.83	0.30	1.02	0.063			0.054	0.001	0.190	1.89
HT-9[c]	0.20	0.52	0.020	0.006	0.22	0.50	11.63	1.00	0.04	0.047	0.08	<0.01		<0.01	0.300	0.52
P91[d]	0.70	0.70			0.40	0.90	8.70	0.70		0.005			0.040		0.200	

[a] Normalization: 46 min at 1066 °C (air cooled), tempered: 42 min at 790 °C (air cooled).
[b] Normalization: 1 h at 1050 °C (air cooled), tempered: 45 min at 770 °C (air cooled).
[c] Normalization: 30 min at 1040 °C (air cooled), tempered: 1 h at 760 °C (air cooled).
[d] P91is the welding filler. Post-weld heat treatment; 3 h at 750 °C (air cooled).

Table 2
Summary of the results obtained from CERT tests in SCW at 400°C to 600°C.

Test condition		Steels	Outlet[a]	Test	YS[b]	MS[c]	E_u[d]	E_{tot}[e]	RA	Fracture
Temp. (°C)	Envi.		conduct.(μS/cm)	duration (hours)	(MPa)	(MPa)	(%)	(%)	(%)	mode
400	Deaerated SCW	T91	0.07	151.5	355 ± 49	415 ± 53	5.5±0.6	12.6±1.3	73.4 ± 6.0	Ductile
		HCM12A	0.07	151.5	460 ± 55	540 ± 60	7.4±0.7	12.2±1.2	53.7 ± 8.4	Ductile
		HT-9	0.07	151.5	490 ± 57	575 ± 62	8.4±0.8	12.1±1.2	51.5 ± 8.5	Ductile, IG
500	Deaerated SCW	T91	0.09	182.2	373 ± 50	392 ± 51	3.2±0.3	14.5±1.5	79.6 ± 5.4	Ductile
		HCM12A	0.09	182.2	397 ± 51	424 ± 53	3.5±0.4	14.8±1.5	74.9 ± 5.7	Ductile
		HT-9	0.09	182.2	471 ± 56	482 ± 56	4.2±0.4	14.4±1.4	63.6 ± 6.6	Ductile, IG
		Weld-T91	0.09	203.0	360 ± 49	375 ± 50	4.5±0.5	15.0±1.5	86.9 ± 4.7	Ductile
		Weld-HCM12A	0.09	203.0	392 ± 51	420 ± 53	5.1±0.5	14.3±1.4	76.5 ± 5.7	Ductile
	100 appb DO	T91	0.13	236.0	345 ± 48	355 ± 49	3.8±0.4	14.0±1.4	73.2 ± 6.1	Ductile
	300 appb DO	T91	0.75	182.0	315 ± 46	335 ± 47	3.1±0.3	11.3±1.1	83.7 ± 4.4	Ductile
		HCM12A	0.75	182.0	335 ± 47	342 ± 48	3.5±0.4	10.9±1.1	77.5 ± 6.5	Ductile
		HT-9	0.75	182.0	410 ± 52	430 ± 53	4.0±0.4	13.9±1.4	70.1 ± 4.9	Ductile, IG
	Ar	T91	N/A	205.0	435 ± 54	470 ± 56	1.2±0.1	15.0±1.5	84.8 ± 5.1	Ductile
		HT9	N/A	205.0	490 ± 57	518 ± 59	2.0±0.2	14.6±1.5	78.5 ± 5.4	Ductile, IG
600	Deaerated SCW	T91	0.10	191.1	155 ± 32	175 ± 34	3.8±0.4	15.3±1.5	60.0 ± 5.9	Ductile
		HCM12A	0.10	191.1	180 ± 35	200 ± 36	4.3±0.4	14.8±1.5	54.2 ± 9.1	Ductile
		HT-9	0.10	191.1	198 ± 36	222 ± 38	4.8±0.5	15.2±1.5	58.2 ± 8.5	Ductile, IG

Note:
[a] Inlet conductivity = 0.06 μS/cm
[b] YS : Yield stress
[c] MS : Maximum stress
[d] E_u : Uniform elongation
[e] E_{tot} : Total elongation

surface of steel). Cracks in HT-9 occurred in three areas of the SCC bars; marked as A, B and C in Fig. 2. These areas are defined by the ratio of the width in the necked region to that in the un-necked region. Area A is from the fracture surface to 80% of the original width, area B is from 80% to 90%, and area C is from 90% to the full un-necked width. Since area A is characterized by extensive localized plastic deformation, no crack analysis was performed in this region. Cracks were recorded and reported only in areas B and C.

3. Results and discussion

Tensile behavior was observed by the stress–strain response examined in CERT tests. SCC was characterized by documenting cracking on the fracture and gage surfaces of the failed specimens. The effects of steel type, temperature and environment on stress–strain behavior will be discussed first, followed by a discussion of fracture behavior.

3.1. Stress–strain behavior

A summary of the results obtained from CERT tests at 400, 500, and 600 °C in DSCW, at 500 °C with 100 and 300 appb DO, and at 500 °C in Ar is presented in Table 2. Plots of stress–strain curves of T91, HCM12A and HT-9 from CERT experiments in DSCW at each temperature are shown in Fig. 3. All of the stress–strain curves showed work-softening behavior. The uniform elongation of these steels ranged between 5% and 10%, and total elongation was 12–15%. There was substantial necking in all samples. The yield strengths were 355–490 MPa for the tests at 400 °C, 375–471 MPa at 500 °C, but only 155–198 MPa at 600 °C. At all temperatures the strengths were in the order HT-9 > HCM12A > T91. Fig. 4 shows a comparison of the stress–strain curves of T91 in different environments at 500 °C, which consists of the tests in Ar, in deaerated SCW, and in SCW containing 100 or 300 appb DO. Note that there is a significant drop in yield strength between Ar and DSCW. With increasing oxygen content in SCW, the yield strength drops

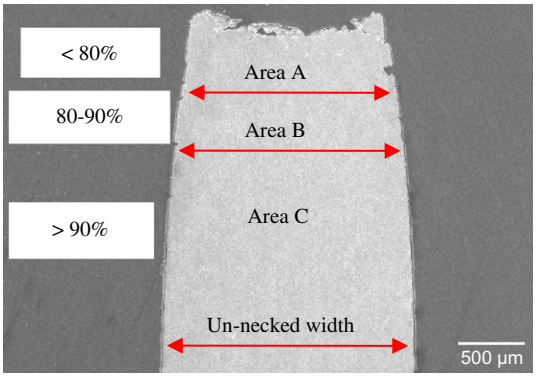

Fig. 2. Areas A, B, and C defined for crack analysis on an HT-9 SCC sample tested in 500 °C and 300 appb DO.

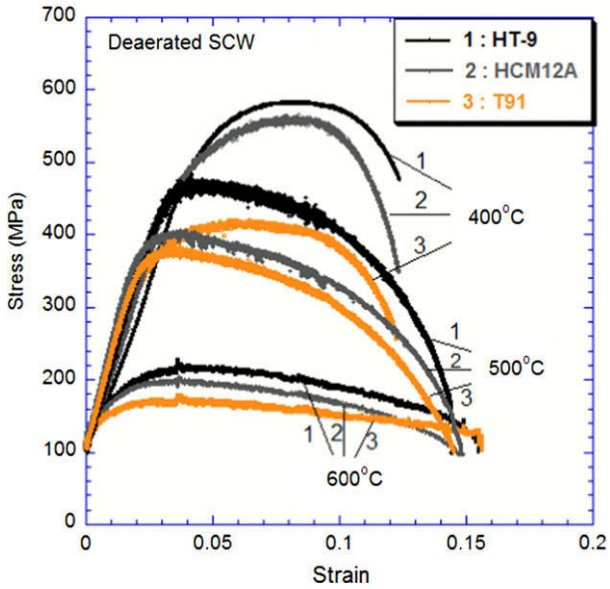

Fig. 3. Engineering stress–strain curves of F–M steels strained in a CERT test at 3×10^{-7} s^{-1} in deaerated SCW at 400, 500 and 600 °C.

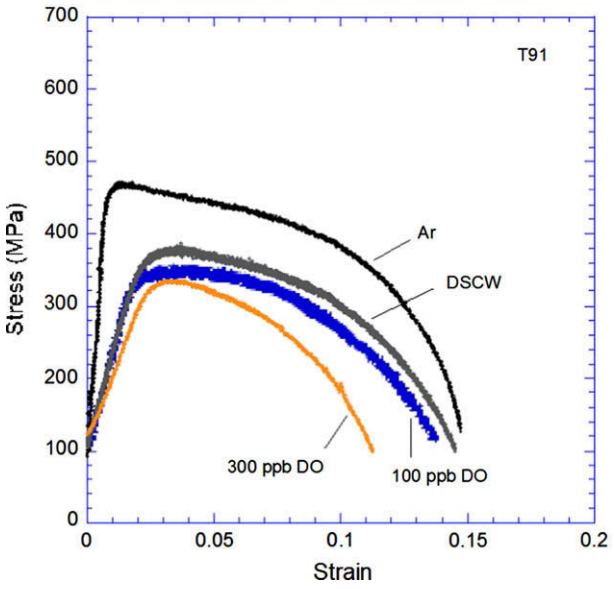

Fig. 4. Engineering stress–strain curves of T91 at 500 °C in Ar, deaerated SCW (DSCW), and SCW containing 100 or 300 appb DO.

slightly and the total elongation decreases more significantly. Comparison of uniform and total elongations is shown in Fig. 5. Comparison of reductions of area (RA) as a function of temperature in DSCW, or as a function of environment at 500 °C is presented in Fig. 6.

3.1.1. Effect of steel composition

Under all conditions, the steels exhibited similar work-softening behavior. For each temperature, HT-9 had the highest yield and maximum stresses, followed by HCM12A, and T91, Fig. 3. The results agree with those reported in the literature [11–13]. The difference in yield strength of steels was governed from several parameters, namely, steel phase, alloying elements, dislocation density, grain size, and particle precipitation. Since these three steels have similar phase (tempered martensite), the difference should be resulted from the other parameters. The grain size has the minor effect in strength since the small grain size steel tends to have the higher yield strength. (In this case, HCM12A has the smallest grain size.) The trend in strength of these F–M steels corresponds to the amount of Cr closely. HT-9 contains the highest amount of Cr (11.67%), followed by HCM12A (10.83% Cr), and T91 (8.37% Cr). Chromium increased strength by the solid solution strengthening. The observed trend is consistent with the work of Bullough et al. [14] where hardening increases with increasing bulk Cr concentration. In addition, chromium and carbon are both important in precipitation strengthening. Since HT-9 has almost twice the amount of carbon (0.2%) as compared to HCM12A (0.1%) and T91 (0.1%), it results in a higher volume fraction of carbides (for example, 3.8 wt.% precipitates in HT-9 as compared to 1.5 wt.% in T91 [15]) precipitated at the PAG and subgrain boundaries. These precipitates act as obstacles to dislocation motion, resulting in higher strength.

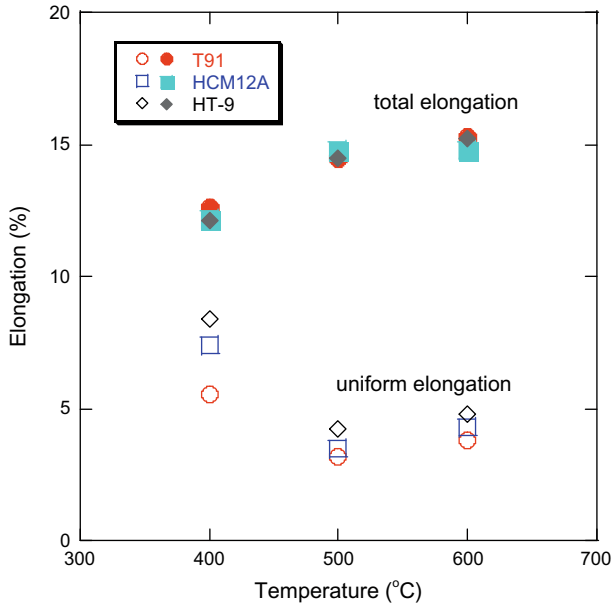

Fig. 5. Uniform and total elongations of T91, HCM12A, and HT-9 at 400–600 °C DSCW.

The three F–M steels exhibited a similar range of total elongation (10–15%) under all test conditions. Low uniform elongation is a typical feature associated with the tempered martensite structure [3]. Although the ductility is similar for the steels tested in each environment, in which T91 has the highest elongation and RA, followed by HCM12A, and HT-9. This behavior in elongation is consistent with the behavior in strength discussed in the preceding paragraph. The low value of elongation in HT-9 may also be due, in part, to intergranular (IG) cracking observed in that steel, as will be discussed in Section 3.3. Fractography showed that all steels failed by ductile rupture. There was no evidence of IG in T91 and HCM12A in any of the test conditions.

3.1.2. Effect of temperature

Temperature has a significant effect on the stress–strain behavior of F–M steels in SCW. Both yield and maximum stresses decreased with increasing temperature, Fig. 3. The trend agrees closely with literature data on typical F–M steels tested at these temperatures [3,11,3]. At higher test temperatures dislocations have a greater mobility as a result of higher thermal energy leading to faster diffusion rate. Also, at high temperatures coarsening of precipitates reduces their strength as obstacles to dislocations [9]. Both of these factors result in easier plastic deformation and thus reduction in strength. They also explain the observed increase in total elongation and RA with rise in test temperature, Figs. 5 and 6.

Uniform elongation (strain to maximum stress) increases as a result of softening, which agrees with results reported by Klueh [16]. However, the decrease in reduction of area in samples tested at 600 °C is unexpected. This could be a result from a lower plastic elongation (defined as the difference between total and elastic elongation) at this temperature, Fig. 5. The plastic deformation in the necked region may have decreased as a result of oxide constraint on the surface, not a behavior of steel. A result on oxidation of F–M steels in SCW [5] showed that oxidation rate increased with increasing temperature. Due to tremendously high oxidation rate at 600 °C, a thick layer of magnetite (Fe_3O_4) ~15–19 μm formed before straining, and rapidly increased with time. Magnetite is harder than the steel substrate (microhardness of magnetite = 345–431 kg/mm^2 [17] and F–M steels = 217–265 kg/mm^2). The oxide can limit the deformation in the transverse direction because it was compressed against the soften substrate [18]. Therefore, the ductility in the transverse direction is decreased. Meanwhile the stress in the tensile direction is high leading to cracks in the oxide, as shown by the cracks on the surface that propagated perpendicular to the tensile direction from one edge to another. Fig. 7 shows a comparison of the high plastic deformation in the necking area of 500 °C sample and the low necking in 600 °C sample. Localized necking was also observed at each crack,

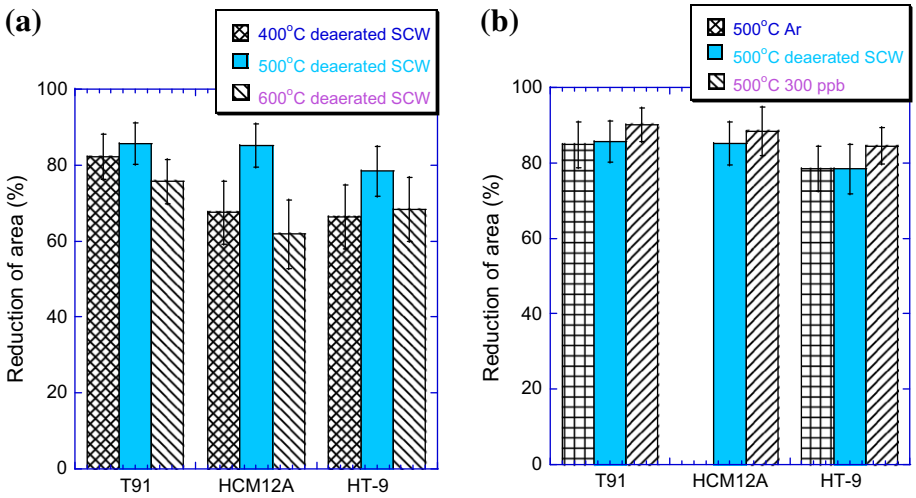

Fig. 6. Comparison of reduction of area (a) at temperature 400, 500, 600 °C DSCW, and (b) at temperature 500 °C in Ar, DSCW, SCW with 300 appb DO.

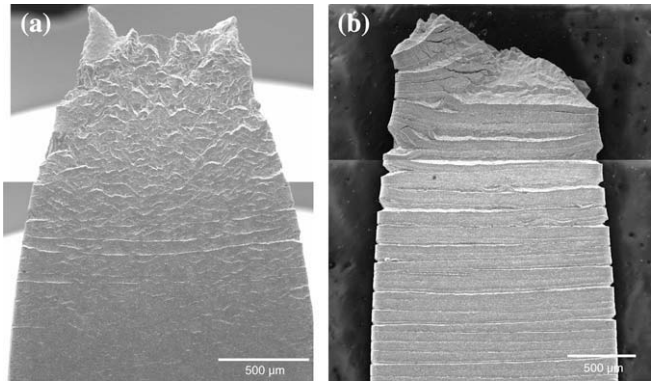

Fig. 7. SEM images of HCM12A tested in deaerated SCW at (a) 500 °C shows high plastic deformation, and (b) 600 °C show low plastic deformation and oxide cracks on the gage section.

implying that the oxide has a significant effect on the reduction of area but not on the yield and maximum stresses of steels.

3.1.3. Effect of the environment and dissolved oxygen

Comparisons of yield stress, maximum stress, elongation, and RA in different environments (Figs. 4 and 6b) show that dissolved oxygen concentration appears to have only a small effect on tensile behavior. Both yield and maximum stresses of T91 and HT-9 were higher in argon as compared to that in the SCW environment, but they still fall in the same range with standard deviation. Total elongation slightly decreased as the DO concentration increased, Fig. 4. These results showed that DO concentration does not have a significant effect on yield and maximum stresses, which is expected. Two significant results observed from the test at 500 °C with 300 appb were the reduction in total elongation for three steels, and the cracking behavior of HT-9. The decrease in total elongation probably was affected from cracking initiated in oxide that formed on the surface, not the behavior of steel. The SCC susceptibility increased at higher oxygen concentration. Further detail about SCC will be discussed in Section 3.3.

3.2. Welded T91 and HCM12A

The welded samples of T91 and HCM12A exhibited values of yield and maximum stresses, total elongation, and RA that were close to those of the base steels tested in the same conditions, Fig. 8. Note that while irradiated samples were used in this comparison, irradiation is not expected to affect the tensile behavior because radiation damage affects only the top 15 μm of the irradiated surface [7], which amounts to less than 1% of the sample cross-section. No cracking was observed in the weld section on both un-irradiated and irradiated sides after CERT tests in SCW, confirming that welding and post-tempering were not affect the susceptibility of cracking.

3.3. Stress corrosion cracking behavior

Among the three F–M steels and the weld samples tested in this study, only HT-9 exhibited IG cracking. The gage surface of HT-9 showed IG cracking in both the necked region and in regions away from the neck. Cross-sections of the gage region were investigated in order to evaluate crack penetration. The maximum crack depth was recorded as this is important in component failure and is a more meaningful characterization of cracking in a small dataset. Cross-section images of crack on HT-9 occurred at 400–600 °C deaerated SCW, and at 500 °C in Ar and 300 appb SCW are showed in Fig. 9. A plot of crack density and maximum crack depth is shown in Fig. 10. The results show that both environment (SCW and DO) and temperature have influence on the crack density and the maximum crack depth.

The effects of environment and DO concentration were determined at 500 °C by performing CERT tests in Ar, in deaerated SCW, and in SCW with 300 appb DO. Results indicate that cracking behavior is influenced by both environment and DO, which the cracking in SCW with 300 appb DO is highest, followed by those in SCW and in Ar. The cracking in Ar is quite low (crack density is ~3 cracks/mm^2 and maximum crack depth is 8.3 μm). However this evidence showed that HT-9 also has susceptibility to IG cracking in non-oxidizing environment. This implied that microstructure of HT-9 plays a role in the inherent susceptibility to IG cracking. The previous work reported by Gupta et al. [9,19] stated that the cracking occurred by either of the following mechanisms; (i) decohesion at the carbide/matrix interface, or (ii) embrittlement due to large PAG size. Therefore HT-9 would be expected to be more susceptible to cracking by virtue of its high carbide precipitate density, and its large PAG size of 4–5 times greater than those of T91 and HCM12A.

The environment has a significant effect to increase the cracking susceptibility from the Ar environment to the deaerated SCW

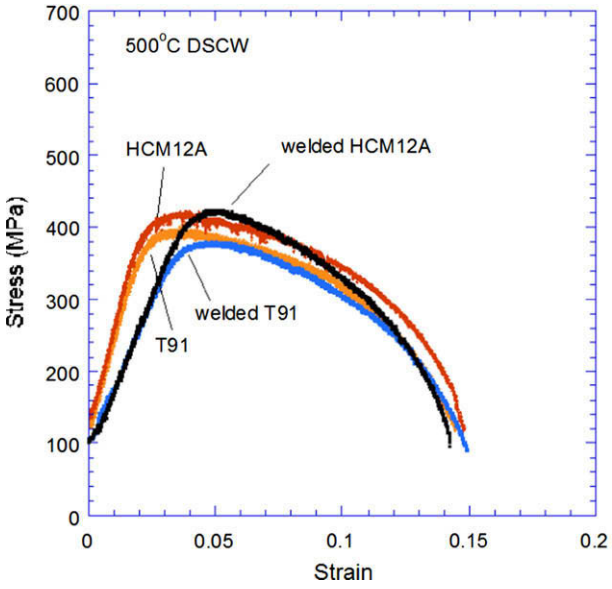

Fig. 8. Engineering stress–strain curves of welded and wrought T91 and HCM12A tested in DSCW at 500 °C.

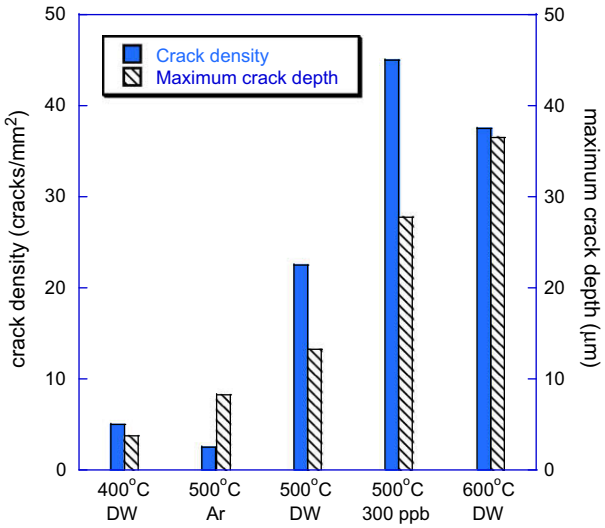

Fig. 10. Crack density and maximum depth of IG cracks on HT-9 tested at 400–600 °C deaerated SCW and at 500 °C in Ar and 300 appb DO SCW.

to the SCW containing 300 appb DO. The trend also follows the oxidation potential of the environment (see [5] for details). Gupta et al. [9,19] described that the environment could influences the cracking during microvoid coalescence at carbide particle and matrix interface. The rapid oxidation of HT-9 steel in SCW occurred by diffusion of cations (Fe or Cr) outward and of anions (O) inward the matrix, which can modify the subsequence plastic flow and the breakage of the alignment between microcracks, thus it promotes additional crack initiation and growth. Observation of oxide grew inside the crack (Fig. 9) also showed that the oxides exerted the pressure to crack tip and induced the crack growth. The result from 300 appb DO SCW test, which the crack density and maximum crack depth increased dramatically, demonstrated that the oxidation generally affected the cracking behavior. Furthermore, note that the crack density of sample tested in 300 appb DO SCW is higher than that in 600 °C deaerated SCW indicating that the oxidation promotes the crack initiation.

Temperature has a major effect on cracking susceptibility in which the crack density is least at 400 °C and highest at 600 °C under deaerated condition. The result of crack density also followed the oxidation potential where oxidation at 600 °C deaerated SCW is the highest [5]. The highest crack depth was observed in 600 °C deaerated SCW (36.5 μm), which covered over half of PAG size of HT-9 (~50 μm). It is important to note that the crack depth was measured from crack tip to interface of outer and inner layer oxide (original steel surface), thus the depth included both crack in inner layer oxide and in matrix. Cracks at 400 and 500 °C deaerated SCW penetrated deep inside the steel matrix while cracks at 600 °C slightly penetrated into the matrix (Fig. 9). Large crack on 600 °C specimen associated with the cracking in oxide since the oxide is very brittle, and it formed thick layers at this temperature. This result also supports that the oxidizing environment of SCW increases the IG cracking susceptibility of HT-9, both for the crack density and the maximum crack depth. However, the microstructure of HT-9 has a major effect on the inherent susceptibility to cracking since two other F–M steels T91 and HCM12A did not crack under the same environment.

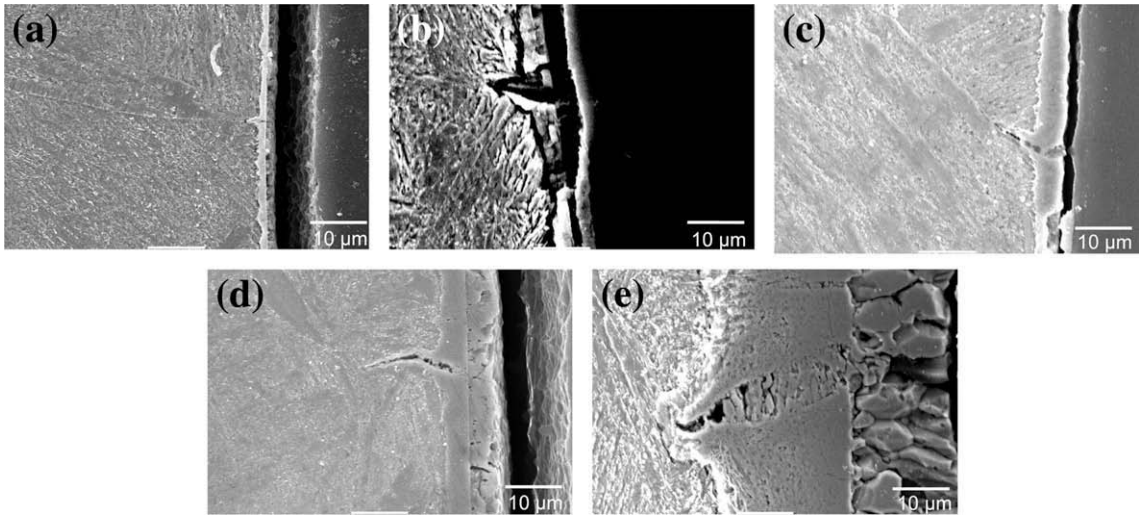

Fig. 9. Cross-section images of crack on HT-9 at (a) 400 °C deaerated SCW, (b) 500 °C in Ar, (c) 500 °C deaerated SCW, (d) 500 °C with 300 appb DO, and (e) 600 °C deaerated SCW. Note that the images may not show the maximum crack depth of each condition.

4. Conclusions

- In CERT tests under all conditions, the yield and maximum stresses for HT-9 are the highest, followed by HCM12A, and T91. RA and total elongation are highest for T91, followed by HCM12A, and HT-9. These trends correspond to the amount of Cr in the steels.
- Temperature has a significant effect on mechanical properties of F–M steels. The yield and maximum stresses decreased rapidly with an increase in test temperature. Conversely, the total elongation increased at higher temperatures. These results are consistent with changes in microstructure at higher temperature; coarsening of carbides and higher dislocation mobility.
- The reductions of area of 600 °C samples are lower than expected. This could be a result of high uniform elongation and low plastic deformation. The formation of a thick oxide layer on the tensile bar limits the deformation in transverse direction.
- The dissolved oxygen concentration in 500 °C test did not show a significant effect on yield and maximum stresses. However, the elongation reduced in 300 appb DO tests.
- Both welded T91 and HCM12A samples tested in 500 °C deaerated SCW exhibited a slight decrease of yield and maximum stresses. This reduction in strength may be a result from the grains coarsening in HAZ. No IG cracking was observed on both weld steels.
- HT-9 was the only steel that displayed evidence of IG cracking. Cracking was observed on both the plastic and uniform deformation regions. Cracks penetrated through both outer and inner oxide layers, and into the steel matrix. Both crack density and maximum crack depth increased with temperature and oxidizing environment. Crack density and depth were highest in 300 appb DO test and lowest in Ar test, implying that increased dissolved oxygen promotes IG cracking susceptibility in HT-9. However the microstructure of the steel plays an important role on the inherent susceptibility to cracking.

Acknowledgements

Support for this work was provided by the United States Department of Energy under the I-NERI project (Contract No. 3F-01041). The authors gratefully acknowledge Dr. James I. Cole of the Idaho National Laboratory for preparation of weld steels in this study. The authors also would like to thank Dr. Sebastien Teysseyre and Josh McKinley for the data of T91 tested in 100 appb DO SCW and valuable input.

References

[1] A Technology Roadmap for Generation IV Nuclear Energy Systems, Report No. GIF002-00, US DOE Nuclear Energy Advisory and the Generation IV International Forum, December 1, 2002 <http://gif.inel.gov/roadmap/pdfs/gen_iv_roadmap.pdf>.
[2] Y. Oka, Nucl. Technol. 109 (1995) 1–10.
[3] R.L. Klueh, D.R. Harries, High Chromium Ferritic and Martensitic Steels for Nuclear Applications, ASTM, Pennsylvania, 2001.
[4] P. Ampornrat, C.B. Bahn, G.S. Was, in: Proceedings of the 12th International Conference on Degradation of Materials in Nuclear Power Systems – Water Reactors, American Nuclear Society, Utah, 2005.
[5] P. Ampornrat, G.S. Was, J. Nucl. Mater. 371 (2006) 1–17.
[6] F. Masuyama, New developments in steels for power generation boilers, in: R. Viswanathan, J.W. Nutting (Eds.), Advanced Heat Resistance Steels for Power Generation, IOM Communications Ltd., London, 1999, pp. 33–48.
[7] G. Gupta, Z. Jiao, A.N. Ham, J.T. Busby, G.S. Was, J. Nucl. Mater. 351 (2006) 162–173.
[8] K.E. Wardle, J.I. Cole, US Depart. Energy J. Undergraduate Res. 3 (2003) 12.
[9] G. Gupta, P. Ampornrat, X. Ren, K. Sridharan, T.R. Allen, G.S. Was, J. Nucl. Mater. 361 (2007) 160–173.
[10] D.J. Paraventi, The Effect of Environment on the Creep Deformation of Ultra-high Purity Ni016Cr–9Fe Alloys at 360 °C, Ph.D. Thesis, University of Michigan, 2000.
[11] R. Viswanathan, W.T. Bakker, in: Proceedings of the 2000 International Joint Power Generation Conference, ASME, Florida, 2000, pp. 1–22.
[12] G.R. Odette, G.E. Lucas, J. Nucl. Mater. 275 (1999) 324–331.
[13] Y. Sawaragi, K. Miyata, S. Yamamoto, F. Masuyama, N. Komai, T. Yokoyama, Properties after service exposure of 2.25Cr–1.6W–V, Nb (HCM12A) steel tubes in a power boiler, in: R. Viswanathan, J.W. Nutting (Eds.), Advanced Heat Resistance Steels for Power Generation, IOM Communications Ltd., London, 1999, pp. 144–156.
[14] R. Bullough, D.R. Harries, M.R. Hayns, J. Nucl. Mater. 88 (1980) 312.
[15] M. Hättestrand, M. Schwind, H.O. Andrén, Microanalysis of 9–12% chromium steels P92 and P122, in: R. Viswanathan, J.W. Nutting (Eds.), Advanced Heat Resistance Steels for Power Generation, IOM Communications Ltd., London, 1999, pp. 199–211.
[16] R.L. Klueh, Int. Mater. Rev. 50 (2005) 287–310.
[17] E.A.G. Shchule, Met. Sci. Heat Treat. 4 (9–10) (1962) 411–413.
[18] P.F. Thomason, Ductile Fracture of Metals, Pergamum Press, UK, 1990.
[19] G. Gupta, G.S. Was, in: Proceedings of the 12th International Conference on Degradation of Materials in Nuclear Power Systems – Water Reactors, American Nuclear Society, Utah, 2005.